Kybernetes

Direct force control for human-machine system with friction compensation

Lie Yu Jianbin Zheng Yang Wang Enqi Zhan Qiuzhi Song

Direct force control for human-machine system with friction compensation

Lie Yu, Jianbin Zheng, Yang Wang and Enqi Zhan
School of Information Engineering, Wuhan University of Technology, Wuhan, China, and
Qiuzhi Song
School of Mechatronical Engineering, Beijing Institute of Technology, Beijing, China

Abstract

Purpose – The purpose of this paper is to present a direct force control which uses two closed-loop controller for one-degree-of-freedom human-machine system to synchronize the human position and machine position, and minimize the human-machine force. In addition, the friction is compensated to promote the performance of the human-machine system.

Design/methodology/approach – The dynamic of the human-machine system is mathematically modeled. The control strategy is designed using two closed-loop controllers, including a PID controller and a PI controller. The frictions, which exist in the rotary joint and the hydraulic wall, are compensated separately using the Friedland's observer and Dahl's observer.

Findings – When human-machine system moves at low velocity, there exists a significant amount of static friction that hinders the system movements. The simulation results show that the system gives a better performance in human-machine position synchronization and human-machine force minimization when the friction is compensated.

Research limitations/implications – The acquired results are based on simulation not experiment.

Originality/value – This paper is the first to apply the electrohydraulic servo systems to both actuate the human-machine system, and use the direct force control strategy consisting of two closed-loop controllers. It is also the first to compensate the friction both in the robot joint and hydraulic wall.

Keywords Direct force control, Friedland observer and Dahl observer, Human-machine force minimization, Human-machine position synchronization, One-degree-of-freedom human-machine system

Paper type Research paper

1. Introduction

Wearable robots have developed rapidly over the last decades and are mainly oriented to assist individuals in a variety of military, medical and industrial applications (Novak and Riener, 2015). A wearable robot is expected to assist force for the wearer in order to reduce the burden on the wearer's body (Lee *et al.*, 2008). Electrohydraulic servo systems (EHSS) widely apply to actuate the wearable robots for their ability to deliver fast, accurate and high-power responses (Mintsa *et al.*, 2012).

However, the wearable robot usually lacks the capability to adequately recognize the actions and intentions of the human wearer. Therefore, to overcome this drawback, various sensors are used by engineers to obtain the command signal from the human wearer such that the robot can be efficiently controlled with the command signal. In many cases, there are mainly two types of sensors, such as position sensors and

Conflict of interest statement: None of these authors has conflict of interest in this research.

Kybernetes
Vol. 45 No. 5, 2016
pp. 760-771

0368-492X
DOI 10.1108/K-08-2015-0205

force sensors, placed on a part of the body but not covered by the wearable robot (Novak and Riener, 2015). The position sensors measure the angle of the robot joint, while the force sensor is used to measure the driving force by actuator or the human-machine force.

The dynamic behavior of an EHSS is highly nonlinear with models involving both the discontinuous sign function and square-root function. The expression for the fluid flow across the servovalve is mainly responsible for the system complexity. Additionally, the values of hydraulic parameters may vary due to temperature changes and air entrapment in the hydraulic fluid. Finally, external disturbances and noise effects result in challenges to ensure precise control of EHSS (Mintsa *et al.*, 2012).

However, a considerable amount of static and dynamic frictions exist in robot joints and sliding surfaces of hydraulic actuator (Tafazoli *et al.*, 1998). The friction presence is often responsible for the inability of the system to achieve low values of steady-state error and may limit the closed-loop bandwidth to avoid limit cycling (Friedland and Park, 1992). The amount of friction changes with time and cannot be readily measured or controlled. Hence, a number of methods are presented to compensate the frictions. Based on various friction models, abundant control schemes have been investigated. Dahl (1968, 1996) developed a simple model to simulate the control systems with frictions. His starting point was experiments on friction in servo systems with ball bearings. Bliman and Sorine (1993a, b) had proposed a number of dynamic models based on the experimental investigations. In their conception, it is assumed that friction only depends on the sign of the velocity and the integration of velocity. The LuGre friction model is a generalization of Dahl's model (Canudas-de-Wit *et al.*, 1995). This model captures many properties of friction such as stiction, rate-dependent friction and frictional lag (Astrom and Canudas-de-Wit, 2008). The model also includes rate dependent friction phenomena such as varying break-away force and frictional lag. On the other side, Friedland and Park (1992) presented an observer to estimate the friction which is modeled as a constant times the sign of the velocity. The observer model is selected to ensure that the error in estimation of the friction constant converges asymptotically to 0.

In this paper, we introduce a one degree-of-freedom (1 DOF) human-machine system, as part of a wearable robot. In order to obtain the command signal from the human wearer, a force sensor is actually located between the human and machine. For simulation, the force sensor is modeled as a spring such that the generating force can be calculated as a product of the difference between the angular positions of the human and machine. Dahl's model and Friedland's model are used to compensate the frictional torque in the robot joint and the frictional force in the hydraulic wall, respectively. In addition, direct force control strategy is proposed which uses two closed-loop controllers to synchronize the human position and machine position, and minimize the human-machine force. The simulation results shows that the system gives a better performance in human-machine position synchronization and human-machine force minimization when the friction is compensated.

2. System modeling

In this section, a dynamic model is derived for the EHSS and 1 DOF human-machine system. This analysis primarily builds the nonlinear model of the actuator (i.e. EHSS) dynamics, and shows the process of the actuator driving the machine. Similar approaches to modeling of hydraulic actuators have been reported in Yao *et al.* (2012, 2013).

The 1 DOF human-machine system under consideration is drafted in Figure 1. The left part of it is the EHSS which mainly consists of the hydraulic and the servo valve. The right part is the human-machine system. The controller design is to make the machine synchronize the human movement, and minimize the human-machine force. In this paper, the human-machine force is measured by a force sensor which is modeled as a spring shown in Figure 1. Additionally, the human-machine force is vertical to the machine body. The total machine dynamics of 1 DOF human-machine system is considered as follows:

$$J\ddot{\theta}_M = T_L + T_{HM} - mgL_g \sin(\theta_M) - T_{f1} - T_{f2} \tag{1}$$

where J is the rotational inertia of the load; θ_M is the rotary angle of the machine; T_L is the actuated torque; T_{HM} is the torque imposed by the human on the machine; m is the machine mass; g is the acceleration due to gravity; L_g is the position of the center of mass of the machine; T_{f1} is the frictional torque in the rotary joint; T_{f2} is the frictional torque in the hydraulic wall.

In this system, the rotary angle (θ_H) of the human is the system input such that the resultant human-machine torque T_{HM} can be modeled as:

$$\begin{cases} T_{HM} = L_{HM} F_{HM} \\ F_{HM} = K_H(\theta_H - \theta_M) \end{cases} \tag{2}$$

where F_{HM} is the human-machine force; L_{HM} is the length from the pivot to the spring; K_H is the impedance between the human and the machine.

On the other side, the torques T_L and T_{f2} can be calculated as:

$$\begin{cases} T_L = (P_1 A_{p1} - P_2 A_{p2})H \\ T_{f2} = F_f H \end{cases} \tag{3}$$

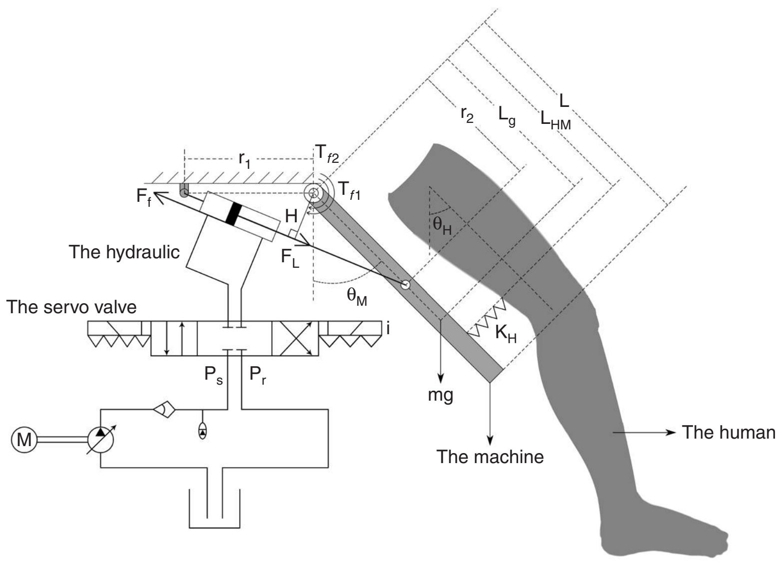

Figure 1.
Schematic diagram of the one-degree-of-freedom human-machine system

where P_1 is the head-side pressure; P_2 is the rod-side pressure; A_{p1} is the head-side area; A_{P2} is the rod-side area; F_f is the frictional force applied on the hydraulic wall. Meanwhile, due to the system geometry, the arm H can be computed as:

$$H = \frac{r_1 r_2 \cos(\theta_M)}{\sqrt{r_1^2 + r_2^2 + 2r_1 r_2 \sin(\theta_M)}} \tag{4}$$

where r_1 and r_2 are the geometric length of the system as drawn in Figure 1.

In Equation (3), the A_{p1} and A_{P2} can be calculated through the following formulas when the bore diameter D_1 and the rod diameter D_2 are acquired:

$$\begin{cases} A_{p1} = \frac{\pi D_1^2}{4} \\ A_{p2} = \frac{\pi\left(D_1^2 - D_2^2\right)}{4} \end{cases} \tag{5}$$

As the rod diameter D_2 is small compared to the bore diameter D_1, Equation (5) can be simplified as:

$$A_{p2} = \frac{\pi\left(D_1^2 - D_2^2\right)}{4} \approx \frac{\pi D_1^2}{4} = A_{p1} \tag{6}$$

Substituting the Equations (4) and (6) into Equation (1), the system model can be simplified as:

$$J\ddot{\theta}_M = P_L A_{P1} H + T_{HM} - mgL_g \sin(\theta_M) - T_{f1} - F_f H \tag{7}$$

where $P_L = P_1 - P_2$ is the load pressure of the dynamic actuator.

As referred to the continuity equation presented by Merritt (1967), through neglecting the external leakage (Yao *et al.*, 2013), the pressure dynamics in actuator chambers can be transformed and described as:

$$\begin{cases} \dot{P}_1 = \frac{\beta}{V_1}\left(-A_{p1} v_p - C_t P_L + Q_1\right) \\ \dot{P}_2 = \frac{\beta}{V_2}\left(A_{p1} v_p + C_t P_L - Q_2\right) \end{cases} \tag{8}$$

where $V_1 = V_0 + A_{p1} x_p$, $V_2 = V_O - A_{p1} x_p$ are the control volumes of the actuator chambers, V_0 chamber volume such that at $x_p = 0$, $V_1 = V_2 = V_0$; β is the effective bulk modulus in the chambers; x_p is displacement of the load; C_t is the coefficient of the total internal leakage of the actuator due to the pressure; Q_1 is the supplied flow rate to the forward chamber and Q_2 is the return flow rate of the return chamber. Q_1 and Q_2 are related to the spool valve displacement of the servo-valve x_v:

$$\begin{cases} Q_1 = k_q x_v \left[s(x_v)\sqrt{P_s - P_1} + s(-x_v)\sqrt{P_1 - P_r}\right] \\ Q_2 = k_q x_v \left[s(x_v)\sqrt{P_2 - P_r} + s(-x_v)\sqrt{P_s - P_1}\right] \end{cases} \tag{9}$$

where:

$$k_q = C_d w \sqrt{\frac{2}{\rho}} \tag{10}$$

s(*) is defined as:

$$s(*) = \begin{cases} 1 & \text{if} * \geq 0 \\ 0 & \text{if} * < 0 \end{cases} \tag{11}$$

where k_q is the valve discharge gain, C_d is the discharge coefficient, w is the spool valve area gradient, ρ is the density of hydraulic oil, P_s is the supply pressure of the fluid, and P_r is the return pressure.

However, x_p and v_p can be calculated as:

$$\begin{cases} x_p = \sqrt{r_1^2+r_2^2+2r_1r_2\sin(\theta_M)}-L_0-x_{p0} \\ v_p = \frac{2r_1r_2\dot{\theta}_M\cos(\theta_M)}{\sqrt{r_1^2+r_2^2+2r_1r_2\sin(\theta_M)}} \end{cases} \tag{12}$$

where L_O is the cylinder dead length and x_{pO} is the piston position when the volumes are equal on both cylinder sides.

Since a high-response servo valve is used, it is assumed that the control applied to the servo valve is directly proportional to the spool position. Then, the following equation is given by $x_v = k_c i$, where k_c is a positive electrical constant, and i is the input current. Thus, from Equation (11), $s(x_v) = s(i)$. Then Equation (9) can be rewritten as:

$$\begin{cases} Q_1 = g_s R_1 i \\ Q_2 = g_s R_2 i \end{cases} \tag{13}$$

where $g_s = k_q k_c$ and:

$$R_1 = s(i)\sqrt{P_s-P_1}+s(-i)\sqrt{P_1-P_r}$$

$$R_2 = s(i)\sqrt{P_2-P_r}+s(-i)\sqrt{P_s-P_2} \tag{14}$$

Based on the Equations (7) and (14), we have:

$$\dot{P}_L = \dot{P}_1-\dot{P}_2 = \left(\frac{R_1}{V_1}+\frac{R_2}{V_2}\right)\beta g_s i-\left(\frac{1}{V_1}+\frac{1}{V_2}\right)\left(\beta C_t P_L+A_{p1}v_p\right) \tag{15}$$

Therefore, the derivation of the actuated force F_L can be obtained by:

$$\dot{F}_L = \dot{P}_L A_{p1} \tag{16}$$

In practical working conditions, P_1 and P_2 are both bounded by P_s and P_r, i.e. $0 < P_r < P_1 < P_s$ and $0 < P_r < P_2 < P_s$. In simulation process, P_L is bounded by P_s, i.e. $-P_s < P_L < P_s$.

3. Friction estimation

The frictional torque T_{f1} and the frictional force F_f in Equation (7) could neither be measured nor accurately modeled. However, one way of dealing with frictions would be to use some of the control observers to compensate the frictions. In order to compensate the frictional force (F_f) in the hydraulic wall, we will particularly focus on the observer-based friction estimation and compensation technique that has been proposed by Friedland and Park (1992). In their presentation, the frictional force F_f in the hydraulic wall can be modeled as a nonlinear and reduced-order observer:

$$\begin{cases} \hat{F}_f = z_f + K_1 x_p + K_2 v_p \\ \dot{z}_f = -K_1 v_p - K_2 \left(F_L - \hat{F}_f \right) \end{cases} \tag{17}$$

where z_f is the observer state; K_1 and K_2 are the observer gains to be chosen to ensure convergence of the error to 0.

As presented in Friedland and Park (1992), in order to ensure convergence of the error to 0, the following conditions must hold:

(1) $K_2 < 0$; and

(2) $d\hat{F}_f/dt$ is bounded.

The frictional torque T_{f1} exists in the machine rotary joint. Joint friction is one of the major limitations in performing high-precision manipulation tasks. It affects both static and dynamic performances, and may cause instability when coupled to position or force feedback control. Therefore, compensation for joint friction has been one of the main research issues in robot design and control over the years (Lischinsky *et al.*, 1999). In this present paper, to compensate joint friction T_{f1}, the Dahl's model (Dahl, 1968, 1996) is selected for its original experiments carried on servo systems with ball bearings. Based on this, the frictional torque T_{f1} can be compensated as:

$$\begin{cases} \frac{dz}{dt} = \theta_M - \frac{\sigma|\theta_M|}{T_c} z \\ \hat{T}_{f1} = \sigma z \end{cases} \tag{18}$$

where z is the observer state; σ is the stiffness coefficient; T_c is the Coulomb frictional force. The magnitude of the estimated frictional torque should never be larger than T_c if its initial value is such that $|T_{f1}(0)| < T_c$.

4. Controller design

From Equations (7) and (16)-(18), the entire system can be expressed in a state-space form as:

$$\begin{cases} \dot{z}_f = K_2 z_f - K_2 F_L + K_1 K_2 x_p + \left(K_2^2 - K_1 \right) v_p \\ \dot{z} = \theta_M - \frac{\sigma|\theta_M|}{T_c} z \\ \dot{\theta}_M = v_M \\ \dot{v}_M = \frac{1}{J}\left(F_L H + T_{HM} - mgL_g \sin(\theta_M) - \left(z_f + K_1 x_p + K_2 v_p \right) - \sigma z \right) \\ \dot{F}_L = f_1 i - f_2 v_p - f_3 F_L \end{cases} \tag{19}$$

where z_f, z, θ_M, v_M and F_L are treated as the system states. As presented in Equation (12), the expressions of x_p and v_p involve the θ_M and the derivative of θ_M (i.e. v_M).

And the f_1, f_2 and f_3 are written as:

$$\begin{cases} f_1 = \left(\frac{R_1}{V_1}+\frac{R_2}{V_2}\right)\beta g_s \\ f_2 = \left(\frac{1}{V_1}+\frac{1}{V_2}\right)A_{p1} \\ f_3 = \frac{1}{A_p}\left(\frac{1}{V_1}+\frac{1}{V_2}\right)\beta C_t \end{cases} \tag{20}$$

In Equation (20), the rotary angle θ_H of the human is the system input while the current i is the system output. In this paper, the control strategy for 1 DOF human-machine system is designed to synchronize the human position and the machine position, and minimize the human-machine force. Therefore, to implement these aims, we design a control strategy with two closed-loop controllers as demonstrated in Figure 2.

In this system, the rotary angle θ_H of the human is the system input which for test purposes is a sinusoidal signal at a sampling frequency of $f_s = 1{,}000$ Hz:

$$\theta_H(t) = 0.4\sin(2\pi f t) \tag{21}$$

As described in Figure 2, the F_{d1} is the desired human-machine force, and f is the motion frequency of the human. One aim of the control strategy is to minimize the human-machine force such that the desired human-machine force F_{d1} is set to be 0:

$$F_e(t) = F_{d1}(t) - F_{HM}(t) = 0 - F_{HM}(t) \tag{22}$$

where F_{HM} is calculated in Equation (2). $F_e(t)$ is the error between the desired and actual human-machine force of the system. Therefore, the PID controller is designed as:

$$F_{d2}(t) = K_{p1}F_e(t) + K_{i1}\int F_e(t)dt + K_{d1}\frac{dF_e(t)}{dt} \tag{23}$$

where K_{p1}, K_{i1} and K_{d1} are the proportional, integral and differential gains, respectively. However, F_{d2} is not only the output of the PID controller but also the input of PI controller:

$$F_i(t) = F_{d2}(t) - F_L(t) \tag{24}$$

where $F_i(t)$ is the error between the desired and actual actuated force of the system. Hence, the PI controller can be described as:

$$i(t) = K_{p2}F_i(t) + K_{i2}\int F_i(t)dt \tag{25}$$

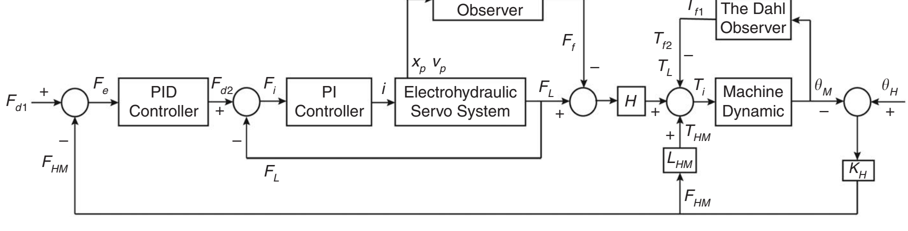

Figure 2.
The block diagram of the control system

where K_{p2} and K_{i2} are the proportional and integral gains, respectively. The system output $i(t)$ is the valve current such that the EHSS generates the force F_L.

5. Simulation results

The ideas have been tested by simulation in Matlab. The parameters of the EHSS and human-machine system are listed in Table I. The gains of the PID and PI controllers are both chosen using Ziegler and Nichols (1942) method. Then, optimum gains of $K_{p1} = 300$, $K_{i1} = 54$ and $K_{d1} = 9$ are used for the PID controller. Meanwhile, optimum gains of for the PI controller are selected that $K_{p2} = 1 \times 10^{-2}$ and $K_{i2} = 1 \times 10^{-3}$. A better description of the friction phenomena is at low velocities and especially crossing zero velocity (Canudas-de-Wit *et al.*, 1995). Based on this, the motion frequency f defined in Equation (21) is chosen to be 1/2.

Tracking performance of the electrohydraulic actuator is investigated through simulation. The computer simulations are conducted for two cases of compensation, such as no friction compensation (NFC) and with friction compensation (WFC). The comparisons of simulation results are shown in Figures 3 and 4. To display the effect of comparison results efficiently, the system performances are indicated by the root-mean-square (RMS) error which is defined in Gomonwattanapanichl *et al.* (2006):

$$RMS\ error = \sqrt{\frac{1}{n}\sum_{1}^{n} (\theta_H - \theta_M)^2} \tag{26}$$

Name	Symbol	Unit	Value
Rotational inertia of the load	J	kg m^2	0.96
Machine mass	m	kg	7
Acceleration due to gravity	g	m/s^2	9.81
Position of the center of mass of the machine	L_g	m	0.24
Length from the pivot to the spring	L_{HM}	m	0.27
Impedance between the human and the machine	K_H	N m/rad	−10
Geometric length of the system	r_1	m	0.04
Geometric length of the system	r_2	m	0.27
Head-side area	A_{p1}	m^2	1.77×10^{-4}
Rod-side area	A_{p2}	m^2	1.57×10^{-4}
Bore diameter	D_1	m	0.015
Rod diameter	D_2	m	0.005
Chamber volume	$V0$	m^3	1.15×10^{-4}
Effective bulk modulus	β	Pa	2×10^7
Coefficient of the total internal leakage	C_t	m^5 N^{-1} s^{-1}	8×10^{-12}
Discharge coefficient	C_d	–	0.61
Spool valve area	w	m^2	9.59×10^{-3}
Valve discharge gain	k_q	m^2 s^{-1}	2.87×10^{-4}
Supply pressure of the fluid	P_s	Pa	2×10^6
Return pressure	P_r	Pa	0.5×10^5
Density of hydraulic oil	ρ	Kg m^{-3}	830
Electrical constant	k_c	m^3 s^{-1} Pa^{-1}	1.38×10^{-4}
Observer gains	K_1	–	−0.9
Observer gains	K_2	–	−0.5
Coulomb frictional torque	T_c	N m	6
Stiffness coefficient	σ	–	3
Cylinder dead length	L_O	m	0.1
Initial piston position	x_{pO}	m	0.08

Table I. System parameters

As the result of RMS error requires n subtractions, n multiplications and n additions ($n \gg 3$), the computational complexity of RMS error is $O(n)$. The comparison in Figure 3 (a) and (b) demonstrates that the system through WFC obtains less RMS error (0.044 rad) than the system through NFC (RMS error = 0.051 rad). According to the RMS values, using WFC results in reduction of the human-machine position error.

To elaborate the comparison result exactly, mean absolute error (MAE) is made to evaluate the effect of human-machine force minimization. In addition, the definition of MAE is made as:

$$MAE = \frac{1}{n}\sum_{1}^{n} |F_{HM}| \tag{27}$$

The result of MAE requires only n additions such that the computational complexity of MAE is $O(n)$. As described in Figure 4, the MAE (9.84 N) of system through WFC is less

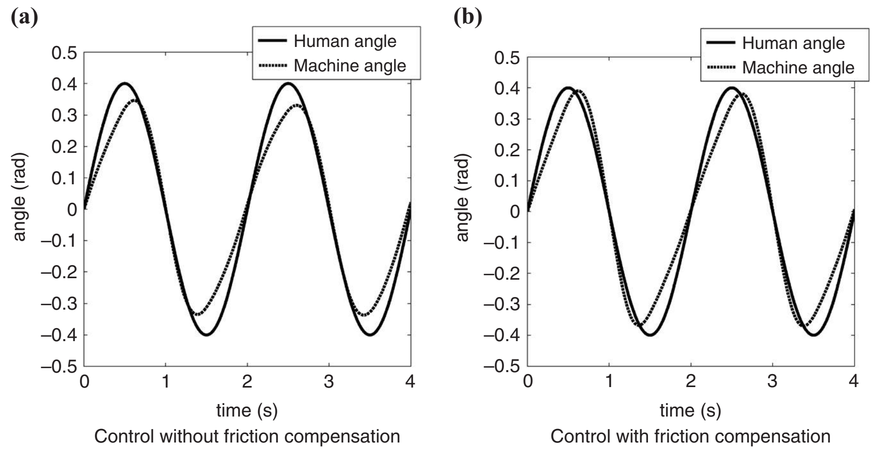

Figure 3. The human-machine position synchronization on the conditions of control with no friction compensation and control with friction compensation

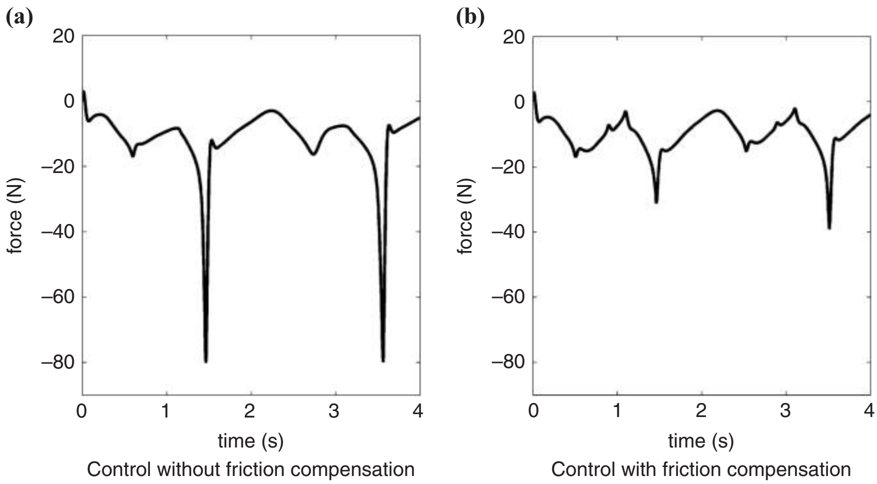

Figure 4. The human-machine force minimization on the conditions of control with no friction compensation and control with friction compensation

than the system through NFC (MAE = 11.89 N). The MAE values show that using WFC results in reduction of the human-machine force error.

The actuated torque T_L, estimated frictional torques T_{f1} and T_{f2} are shown in Figure 5. According to this figure, there exists a significant amount of static friction that affects the machine movements. From the results of Figures 3 and 4, it is clear that the effect of friction is suppressed by the proposed friction compensation strategy.

Finally, a comparison simulation was made to test the performance of each friction observer. At first, only the friction existing in the hydraulic wall was compensated. In this situation, the value of RMS error is 0.049 rad while the value of MAE is 11.38 N. Second, we only compensated the friction existing in the robot joint with the result that the value of RMS error is 0.046 rad while the value of MAE is 10.05 N. As described in Table II, the comparison results show that friction compensation for both places (i.e. the hydraulic wall and robot joint) gives better performance than that for only one place.

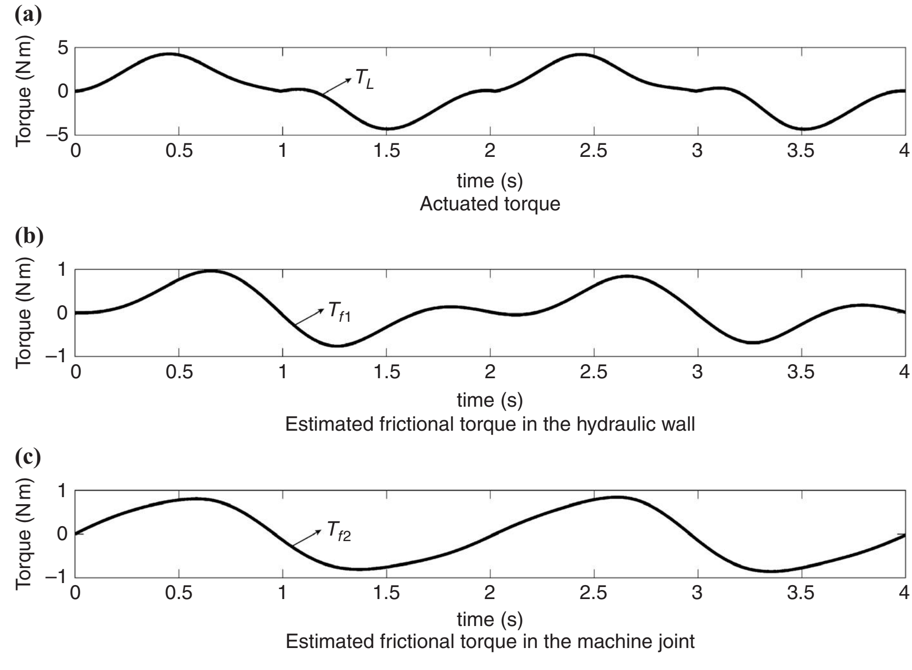

Figure 5. The actuated torque and estimated frictional torques

The friction compensation	RMS error of human-machine position (rad)	MAE of human-machine force (N)
No friction compensation	0.051	11.98
Only in the hydraulic wall	0.049	11.38
Only in the machine joint	0.046	10.05
Both in the hydraulic wall and machine joint	0.044	9.84

Table II. Comparison of friction compensation

6. Conclusion

Direct force control for 1 DOF human-machine system, under the actuation of EHSS, was considered in this paper. The control strategy consists of two closed-loop controllers, including a PID controller and a PI controller, to synchronize the human and machine positions, and minimize the human-machine force. The frictions existing in the rotary joint and the hydraulic rod are severally compensated using Friedland's and Dahl's observers. The simulation results showed that the system control WFC gives a better performance in human-machine position synchronization and human-machine force minimization.

Except for the simulation modeling, the real human-machine system has been built to carry out the experiments of human-machine synchronization. In real system, the human-machine force is measured by a multi-axis force/torque sensor, while the measurement of the machine position is achieved by an encoder mounted in the machine joint. In addition, the driving force generated by EHSS is acquired by a pull-push sensor which can measure both the pull and push forces. However, the human position is not necessary to be obtained because the human and machine joints are banded together. Using the proposed control strategy, the aim has been implemented that the human and machine joints move in synchronization, while the human-machine force is negligible when compared with the driving force. In the future, the friction compensation experiments will be carried out to verify the simulation results in this paper.

References

Astrom, K.J. and Canudas-de-Wit, C. (2008), "Revisiting the LuGre friction model", *IEEE Control Systems Magazine*, December, pp. 101-114.

Bliman, P.A. and Sorine, M. (1993a), "Friction modeling by hysteresis operators application to Dahl' stiction and Stribeck effects", Models of Hysteresis, Pitman Research Notes in Mathematics Series No. 286, Longman Scientific and Technical, Harlow, pp. 10-19.

Bliman, P.A. and Sorine, M. (1993b), "A system theoretic approach of systems with hysteresis application to friction modeling and compensation", *Proceedings of the Second European Control Conference*, pp. 1844-1849.

Canudas-de-Wit, C., Olsson, H., Astrom, K.J. and Lischinsky, P. (1995), "A new model for control of systems with friction", *IEEE Transactions on Automatic Control*, Vol. 40 No. 3, pp. 419-425.

Dahl, P.R. (1968), "A solid friction model", Tech. Rep. TOR-0158, The Aerospace Corporation, El Segundo, CA, pp. 3107-3118.

Dahl, P.R. (1996), "Solid friction damping of mechanical vibrations", *AIAA Journal*, Vol. 14 No. 12, pp. 1675-1682.

Friedland, B. and Park, Y.J. (1992), "On adaptive friction compensation", *IEEE Transactions on Automatic Control*, Vol. 37 No. 10, pp. 1609-1612.

Gomonwattanapanichl, O., Pattanapukdee, A. and Mongkolwongrojn, M. (2006), "Compensation and estimation of friction by using extended Kalman filter", *SICE-ICASE International Joint Conference*, *October 18-21*, pp. 5032-5035.

Lee, H.D., Yu, S.N., Lee, S.H., Han, J.S. and Han, C.S. (2008), "Development of human-robot interfacing method for assistive wearable robot of the human upper extremities", *SICE Annual Conference*, *August*, pp. 1755-1760.

Lischinsky, P., Canudas-de-Wit, C. and Morel, G. (1999), "Friction compensation for an industrial hydraulic robot", *IEEE Control Systems*, Vol. 19 No. 1, pp. 25-32.

Merritt, H.E. (1967), *Hydraulic Control Systems*, John Wiley & Sons, New York, NY.

Mintsa, H.A., Venugopal, R., Kenne, J.P. and Belleau, C. (2012), "Feedback linearization-based position control of an electrohydraulic servo system with supply pressure uncertainty", *IEEE Transactions on Control Systems Technology*, Vol. 20 No. 4, pp. 1092-1099.

Novak, D. and Riener, R. (2015), "A survey of sensor fusion methods in wearable robotics", *Robotics and Autonomous Systems*, Vol. 73 No. 1, pp. 155-170.

Tafazoli, S., W-de-Silva, C. and Lawrence, P.D. (1998), "Tracking control of an electrohydraulic manipulator in the presence of friction", *IEEE Transactions on Control System Technology*, Vol. 6 No. 3, pp. 401-411.

Yao, J.Y., Jiao, Z.X. and Han, S.S. (2013), "Friction compensation for low velocity control of hydraulic flight motion simulator: a simple adaptive robust approach", *Chinese Journal of Aeronautics*, Vol. 26 No. 3, pp. 814-822.

Yao, J.Y., Jiao, Z.X. and Yao, B. (2012), "Robust control for static loading of electro-hydraulic load simulator with friction compensation", *Chinese Journal of Aeronautics*, Vol. 25 No. 6, pp. 954-962.

Ziegler, J.G. and Nichols, N.B. (1942), "Optimum settings for automatic controllers", *Transactions of the ASME*, Vol. 64 No. 1, pp. 759-768.

Corresponding author
Yang Wang can be contacted at: powerflow@whut.edu.cn